Hindawi Publishing Corporation
Mathematical Problems in Engineering
Volume 2013, Article ID 989237, 10 pages
http://dx.doi.org/10.1155/2013/989237

Research Article

Numerical Investigation of Flow and Heat Transfer in a Dimpled Channel among Transitional Reynolds Numbers

Huancheng Qu, Zhongyang Shen, and Yonghui Xie

School of Energy and Power Engineering, Xi'an Jiaotong University, Xi'an, Shaanxi 710049, China

Correspondence should be addressed to Yonghui Xie; yhxie@mail.xjtu.edu.cn

Received 8 October 2013; Revised 9 November 2013; Accepted 11 November 2013

Academic Editor: Gongnan Xie

The SST turbulent model coupled with Gamma-Theta transition model was adopted in the investigation of the flow and heat transfer characteristics of a rectangular channel with arrays of dimples among transitional Reynolds number. The results show that the velocity gets plumper along streamwise direction which indicates that the flow is transited from laminar flow to turbulent flow, which is also confirmed by the turbulence intermittency distribution. The dual vortex inside the dimple becomes asymmetrical when Reynolds number increases. The averaged Nusselt number decreases monotonously in the streamwise direction when the flow is under laminar condition while it increases monotonously when the flow is under turbulent condition. The heat transfer is enhanced by the dimple when the flow is turbulent and it increases with the dimple depth. However, the heat transfer is worsened by the dimple when the flow is laminar. The friction factor increases when the dimple depth increases. The overall thermal performance increases with Reynolds number. The dimple arrays with depth ratio equal to 0.2 show the best overall thermal performance.

1. Introduction

A wide range of industrial applications involve heat transfer problems including the cooling of gas turbine blades, combustion chamber and high-pressure disk, printing of circuit boards, cooling of microelectronic components, and drying of papers and textiles. Heat transfer enhancement and flow resistance reduction are one of the most effective measures in the energy conservation and a great deal of effort has been put into the heat transfer augmentation with minimal pressure drop penalty in recent years.

Dimple is one kind of concavity which has a significant enhancement in heat transfer with low penalty in pressure drop. Terekhov et al. [1] conducted the experimental investigation on the heat transfer and aerodynamic resistance of a single dimple (h/D = 0.33, δ/D = 0.13–0.5, Re_D = 10000–70000) with sharp and round edge. The heat transfer enhancement of shallow dimple is caused both by auto oscillations generated by the cavity and the increase in the surface of dimple while the heat transfer augment of deep dimple is mainly caused by the increase in the surface of dimple. Pressure loss decreases with increase of Reynolds number and the value for round edge dimple is only half of that for sharp edge dimple. Arrays of hemispheric and teardrop shaped dimples (h/D = 0.33–2, δ/D = 0.25, Re_D = 10000–50000) were adopted and compared by Chyu et al. [2] using automated liquid crystal imaging system. Both of the two types of dimple arrays induce heat transfer enhancement of about 2.5 times their smooth cases, which are comparable to most of the rib turbulator while the pressure losses is just half of that with rib turbulator.

The channel height effect on heat transfer and friction in a rectangular channel with dimple arrays (h/D = 0.37–1.49, δ/D = 0.13, $\mathrm{Re}_{\mathrm{HD}}$ = 12000–60000) was experimentally investigated by Moon et al. [3] using a transient thermochromic liquid crystal technique. The flow structure of a channel with a dimpled surface on one wall, both with and without protrusions on the other wall (h/D = 0.5, δ/D = 0.2, Re_h = 380–30000), was studied by Ligrani et al. [4]. The effect of inlet turbulent intensity level, dimple depth, and shape on the flow and heat transfer of a dimpled surface was also investigated by Ligrani et al. [5–9]. The heat transfer augment increases with the dimple depth when the Reynolds number varies from 9540 to 74800 and the local Nusselt

number shows a slight decrease as the inlet turbulent intensity increases.

Heat transfer and pressure drop in different sets of dimpled fin channels including protrusion-dimple channel, dimple-dimple channel, and protrusion-protrusion channel (h/D = 1.0, δ/D = 0.3, Re_h = 1500–11000) were experimentally examined by Chang et al. [10]. Heat transfer coefficient and friction factor for channel with dimples and protrusions installed on single or both wall (h/D = 1.15, δ/D = 0.29, $\mathrm{Re}_{\mathrm{HD}}$ = 1000–10000) were acquired by Hwang et al. [11], and the result shows that the thermal performance is high at lower Reynolds number and the value is about 6.5 and 6.0 for the double protrusion and dimple wall for $\mathrm{Re}_{\mathrm{HD}}$ = 1000, respectively. A complementary investigation with experiment and numerical method about the drag reduction of dimple (h/D = 3.33, δ/D = 0.05, Re_h = 21870–87480) was conducted by Lienhart et al. [12], and it shows that the heat transfer augmentation is feasible to achieve by shallow dimples without significant pressure losses. Kore et al. [13] also experimentally conducted the investigation into the heat transfer performance on the dimpled surface in a channel (h/D = 0.5, δ/D = 0.2–0.4, Re_h = 6250–25000) and the optimal dimple depth was obtained with the maximum heat transfer and thermal performance.

The dimples as well as protrusions and pins were applied in the internal blade tip-wall by Xie et al. [14, 15] to predict the heat transfer enhancement with δ/D = 0.5, Re_h = 100000–600000. The numerical results indicate that the structures adopted improve the overall performance of heat transfer. Chen et al. [16] numerically studied the heat transfer of turbulent channel flow over dimpled surface (h/D = 0.4, δ/D = 0.05–0.2, Re_h = 4000–6000). The study of flow and heat transfer in channels with pin fin-dimple combined arrays (h/D = 1.0, δ/D = 0.2, Re_h = 8200–54000) was conducted experimentally and numerically by Rao et al. [17–19] as well as the effect of dimple depth on the heat transfer in pin fin-dimple channels (h/D = 1.0, δ/D = 0.1–0.3, Re_h = 8200–80800). The dimples distinctively enhance the heat transfer in the pin fin cases and increase the near-wall turbulent mixing level. Angled ribs and dimples were coupled (h/D = 4.17–8.33, δ/D = 0.191, $\mathrm{Re}_{\mathrm{HD}}$ = 30000–50000) and the heat transfer coefficients were measured experimentally by Choi et al. [20]. The dimples further increase the thermal performance compared with that for rib only or dimple only cases. Minichannel with dimples, cylinder grooves, and low fins were adopted in [21] (h/D = 2, δ/D = 0.4, $\mathrm{Re}_{\mathrm{HD}}$ = 2700–6100).

Most of the above works involve the turbulent flow in the channel with dimples. And the dimple shows better heat transfer performance in the comparison with ribs pin fins. However, the flow is laminar when the velocity is very low or the structure is in micro-/miniscale. Xiao et al. [22] experimentally investigated the thermal performance of dimpled surface in laminar flows (h/D = 0.25–0.5, δ/D = 0.1–0.3, Re_h = 260–1030), and the result shows that the heat transfer enhancement is lower for smaller channel height for the same Reynolds number. The flow and heat transfer performance in a microchannel with dimple/protrusion (h/D = 0.5, δ/D = 0.2, Re_h = 100–900) was studied by Lan et al. [23] and water was used as the working fluid.

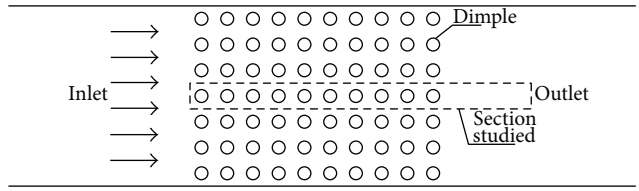

Figure 1: Side view of the dimpled passage.

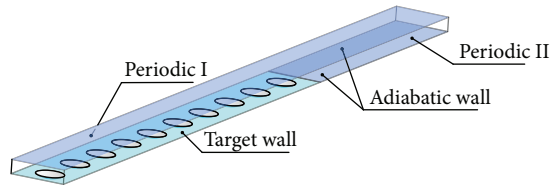

Figure 2: 3D view of the computational region with boundary condition.

Up to now, the works about the heat transfer enhancement with dimple focuse on the turbulent conditions or laminar conditions. The boundary layer was transited more easily by the dimple in low Reynolds number and the heat transfer could show different trends when the transitional Reynolds number occurs. The present investigation reports the numerical simulation of transitional flow and heat transfer in a channel with dimples. The depth of dimple varies from 0.1 to 0.3 and the Reynolds number based on the height of channel changes from 1000 to 5000.

2. Physical Model

The physical situation considered in the present research is illustrated in Figure 1. There are ten dimple arrays in the streamwise direction as well as seven dimple arrays in the cross-section. For getting a more accurate numerical result with dense grid, the single dimple array in the center streamwise direction was chosen as the research domain as marked by the dashed line in Figure 1.

The 3D view and the center section of the computational region are shown in Figures 2 and 3, respectively. The target surface was arranged with ten dimples in the streamwise direction, and constant heat flux q was applied on the target surface with dimple. The wall between target surface and outlet was set as the adiabatic as well as the top wall. All the walls were nonslip in the computation. Periodic boundary conditions were employed on both sides of the dimple array, which are named periodic I and periodic II as shown in Figure 2. Fully developed velocity was used for inlet boundary condition as shown in Figure 3(a) and its magnitude was set on the basis of Reynolds number. The pressure outlet was set as the atmospheric pressure. The channel height was set as h/D = 0.5 and the dimple depth δ/D varied from 0.1 to 0.3 depicted in Figure 3(b). In order to describe the flow and heat transfer performance inside

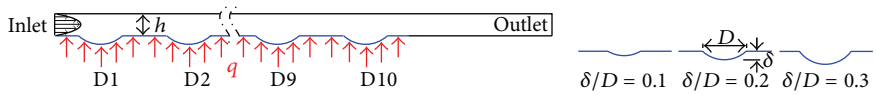

(a) The center section of the computational region (b) Dimple depth

FIGURE 3: Schematic diagram of the 2D domain and the geometric parameters.

different dimple regions in the streamwise direction, the dimples were numbered successively as $D(i)$, $i = 1, \ldots, 10$ which is shown in Figure 3(a).

The Reynolds number based on the height of the channel is defined as

$$\mathrm{Re} = \frac{\rho U h}{\mu}, \tag{1}$$

where ρ and μ are the density and molecular viscosity, respectively. U is the average velocity in the upstream of dimple.

The Nusselt number is defined as

$$\mathrm{Nu} = \frac{q}{\Delta T} \cdot \frac{h}{\lambda}, \tag{2}$$

where ΔT is the averaged temperature difference between fluid and target wall. λ is the thermal conductivity. Consider

$$\Delta T = \frac{\left(T_{w,\mathrm{inlet}} - T_{f,\mathrm{inlet}}\right) - \left(T_{w,\mathrm{outlet}} - T_{f,\mathrm{outlet}}\right)}{\ln\left[\left(T_{w,\mathrm{inlet}} - T_{f,\mathrm{inlet}}\right) / \left(T_{w,\mathrm{outlet}} - T_{f,\mathrm{outlet}}\right)\right]}, \tag{3}$$

where $T_{w,\mathrm{inlet}}$, $T_{f,\mathrm{inlet}}$, $T_{w,\mathrm{outlet}}$, and $T_{f,\mathrm{outlet}}$ are the wall and fluid temperatures at the inlet and outlet boundary, respectively. The corresponding temperatures in the upstream and downstream are chosen for each dimple region in the definition of the averaged Nusselt number in different dimple regions.

The Fanning friction factor is described as

$$f = -\frac{(\Delta p / L)\, h}{2\rho U^2}, \tag{4}$$

where Δp is the averaged pressure difference between inlet and outlet. L is the length of region considered.

The thermal performance is defined as

$$\mathrm{TP} = \left(\frac{\mathrm{Nu}}{\mathrm{Nu}_0}\right) \cdot \left(\frac{f}{f_0}\right)^{-1/3}, \tag{5}$$

where Nu_0 and f_0 are the Nusselt number and Fanning friction factor in the corresponding flat target surface cases, respectively. In the present study, Nu_D and Nu_{D0} are the averaged Nusselt number on each dimple region in dimple case and the corresponding flat target region in flat case, respectively. $\mathrm{Nu}_{\mathrm{OA}}$, f_{OA}, $\mathrm{Nu}_{\mathrm{OA0}}$, and f_{OA0} are the overall averaged Nusselt number and friction factor on the whole target surface in dimple case and the corresponding flat case, respectively.

3. Numerical Method

3.1. Governing Equations. The flow and heat transfer characteristics were analyzed by solving the 3D Navier-Stokes (N-S) equations. The computational work was carried out by using the commercial software ANSYS CFX. The resulting conservation equations of mass, momentum, and energy are given by

$$\begin{aligned}
&\frac{\partial \rho}{\partial t} + \frac{\partial \rho u_i}{\partial x_i} = 0,\\
&\frac{\partial \rho u_i}{\partial t} + \frac{\partial \rho u_i u_j}{\partial x_i} = \rho g_i + F_i - \frac{\partial P}{\partial x_i} + \frac{\partial}{\partial x_i}\left(2\mu S_{ij}\right),\\
&\frac{\partial \rho E_0}{\partial t} + \frac{\partial \rho u_i E_0}{\partial x_i} = \rho u_i F_i - \frac{\partial q_i}{\partial x_i} + \frac{\partial}{\partial x_i}\left(u_i T_{ij}\right),
\end{aligned} \tag{6}$$

where t, x, u, g, and P represent time, coordinate, velocity, acceleration of gravity, and pressure, respectively. F, T, E, and S are body force, surface force, total internal energy, and strain rate tensor, respectively. $i, j = 1, 2, 3$.

3.2. Turbulence Model. In the present Reynolds number ranges, the laminar boundary layer is separated by the dimple and it gets into turbulent flow by boundary layer transition. The shear stress transport (SST) turbulence model [24] coupled with Gamma-Theta transition model [25] is considered as a more effective method to solve the transition flow in the computational study. The transport equations for intermittency γ and transition momentum thickness Reynolds number $\mathrm{Re}_{\theta t}$ are defined as follows:

$$\begin{aligned}
&\frac{\partial(\rho\gamma)}{\partial t} + \frac{\partial(\rho u_i \gamma)}{\partial x_i} = P_{\gamma 1} - E_{\gamma 1} + P_{\gamma 2} - E_{\gamma 2} + \frac{\partial}{\partial x_i}\left[\left(\mu + \frac{\mu_t}{\sigma_f}\right)\frac{\partial \gamma}{\partial x_i}\right],\\
&\frac{\partial(\rho \mathrm{Re}_{\theta t})}{\partial t} + \frac{\partial(\rho u_i \mathrm{Re}_{\theta t})}{\partial x_i} = P_{\theta t} + \frac{\partial}{\partial x_i}\left[\sigma_{\theta t}(\mu + \mu_t)\frac{\partial \mathrm{Re}_{\theta t}}{\partial x_i}\right],
\end{aligned} \tag{7}$$

where $P_{\gamma 1}$ and $E_{\gamma 1}$ are the transition sources and $P_{\gamma 2}$ and $E_{\gamma 2}$ are the destruction sources. $P_{\theta t}$ is the source term for the transition momentum thickness Reynolds number. The intermittency is used to turn on the production terms of the turbulent kinetic energy downstream of the transition point. The transition momentum thickness Reynolds number induces the empirical correlations and captures the influence of the turbulence kinetic energy and adverse pressure gradient in the freestream. The transition model is built on local

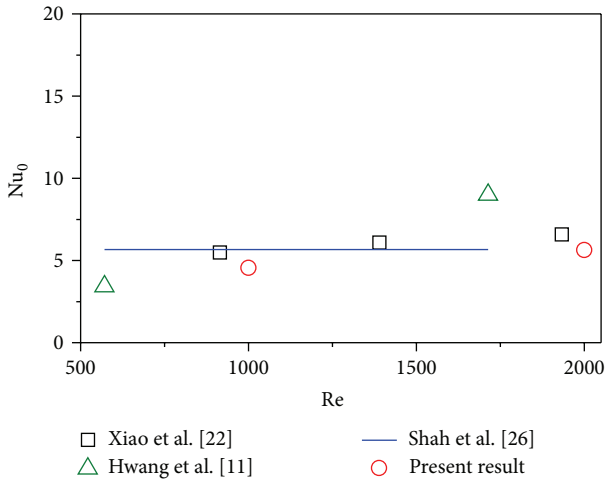

FIGURE 4: Validation of numerical method adopted.

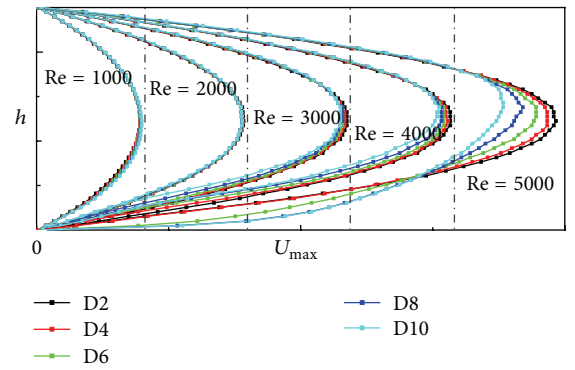

FIGURE 5: The velocity profile along the height direction in different dimple regions when $\delta/D = 0.1$.

variables and is achieved easily with CFD methods. Moreover, based on the experimental data, the transition model can predict variable transition process using proper formula. The transition model couples with the SST turbulence model in the present study. k-w model is solved in the near boundary layer while k-ε model is solved in the freestream in the SST turbulence model. It has the advantages of both k-w and k-ε, which is more accurate for the flow with advanced pressure gradient and shock wave:

$$\begin{aligned}
\frac{\partial(\rho k)}{\partial t} + \frac{\partial(\rho u_i k)}{\partial x_i} &= \overline{P}_k - \overline{D}_k + \frac{\partial}{\partial x_i}\left[(\mu + \sigma_k \mu_t)\frac{\partial k}{\partial x_i}\right], \\
\frac{\partial(\rho \omega)}{\partial t} + \frac{\partial(\rho u_i \omega)}{\partial x_i} &= \alpha \frac{P_k}{\nu_t} - D_\omega + Cd_\omega \\
&\quad + \frac{\partial}{\partial x_i}\left[(\mu + \sigma_k \mu_t)\frac{\partial \omega}{\partial x_i}\right], \\
\overline{P}_k &= \gamma_{\text{eff}} P_k, \\
\overline{D}_k &= \min\left[\max\left(\gamma_{eff}, 1.0\right)\right] D_k.
\end{aligned} \tag{8}$$

The numerical method adopted in the present investigation was validated by different experimental data from [11, 22, 26]. The averaged Nusselt number of fully developed section in flat region Nu_0 was compared in Figure 4. The present result shows the same level as the experimental result. Although there exists a difference which mainly results from that the dimensions of the channel vary in the experiments, the numerical method adopted is in accordance with the experiment.

3.3. Grid Independence Validation. The grid should have a y^+ of approximately 1 for capturing the laminar and transition flow in the SST turbulence model coupled with Gamma-Theta transition model. So the y^+ is less than 1 in all the involved computational cases. The grid independence validation was performed in the flat target surface with Re = 3000. Four different sets of grid were adopted and a constant grid refinement ratio $r = 1.3$ was employed in the three directions. The detailed validation between different sets was shown in Table 1. The relative deviations of the overall averaged Nusselt number and friction factor between adjacent sets of grid decrease gradually with the increase of nodes. The lowest relative deviations of the overall averaged Nusselt number and friction factor are 0.85% and 0.20 between the sets of grid with 4886955 and 10456820 nodes. So the set of grid with 4886955 nodes was chosen with the aim to reduce the computation and maintain the precision.

4. Result and Discussion

4.1. Flow Characteristics. The velocity is fully developed at the inlet boundary. However, the velocity boundary layer will be disturbed by the dimple arrangement and the impact is different along streamwise direction. The velocity profile along the height direction in front of different dimple regions when $\delta/D = 0.1$ is illustrated in Figure 5. For the brevity of the description and explanation, the dimple regions D2/D4/D6/D8/D10 are chosen. The velocity along height direction is almost the same as streamwise position changes when Reynolds number is lower than 3000. It shows that the flow is not affected by the dimple arrangement. However, the velocity shows different trends when the Reynolds number is above 3000. The maximum magnitude of velocity decreases significantly along streamwise direction. The velocity profile shows plumper and gets into turbulent boundary layer condition along streamwise direction.

Turbulence intermittency describes the flow pattern between laminar flow and turbulent flow. Figure 6 shows the turbulence intermittency contours and the streamline distribution when $\delta/D = 0.1$. The flow is laminar when the turbulence intermittency is near zero as shown in D2/D6/D10 when Re = 1000. However, the transition happened above the dimple and the turbulence increases wholly when Re = 3000. When the Reynolds number is 5000, the flow above the dimple D2 is transited and the flow in the D6/D10 is almost fully turbulent. The flows both in D6 and D10 are similar, which indicates that the flow is fully developed in

Table 1: Grid independence validation.

Set of grid	Nodes	Nu_{OA0}	Difference%	$f_{OA0} \times Re$	Difference%
1	984825	13.45	2.96	47.57	8.68
2	2262085	13.86	1.56	43.77	0.61
3	4886955	14.08	0.85	44.04	0.20
4	10456820	14.20	/	43.95	/

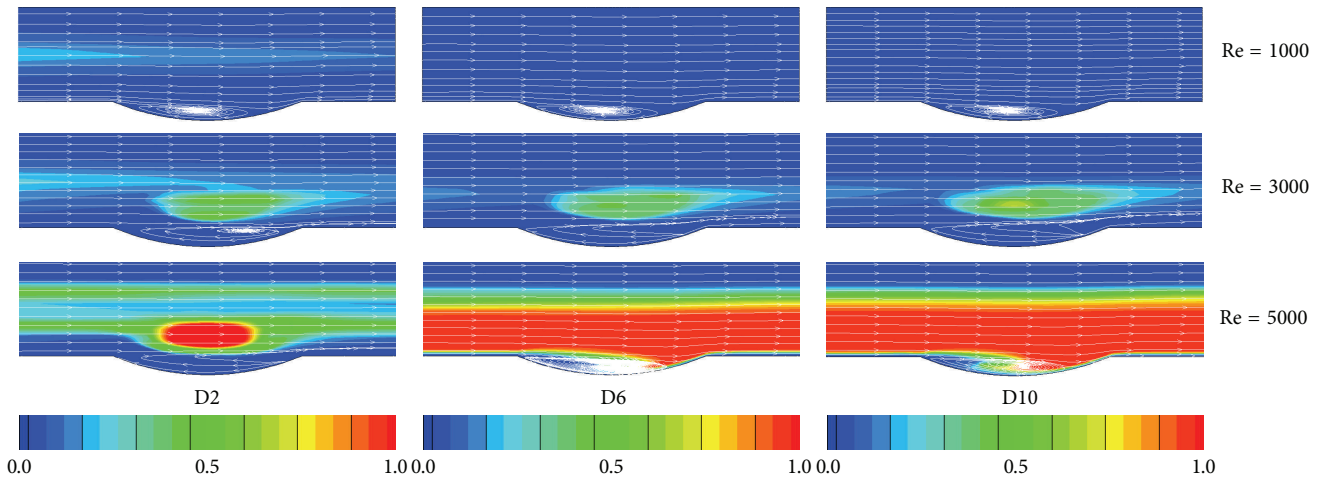

Figure 6: Turbulence intermittency contours and the streamline distribution when $\delta/D = 0.1$.

the streamwise direction from the D6 region in different Reynolds numbers.

Since the flow is fully developed from the D6 region in streamwise direction, the last dimple D10 was chosen as the key region in the present investigation. The limiting streamline and the temperature distributions on the dimple D10 surface are shown in Figure 7 with different dimple depths and Reynolds numbers. The flow characteristics in the dimples are perfectly symmetrical when the dimple depth is 0.1. The flow recirculation is significantly visible inside the dimple. The flow separates in the upstream edge of the dimple and reattaches in the downstream of the dimple. One large vortex is observed inside the dimple when Re = 1000 and $\delta/D = 0.1$. However, the symmetrical dual vortices appear when the Reynolds number increases. From the comparison of temperature between different regions, the temperature of flow separation region shows high values while the flow reattachment region and the trailing edge dimple show lower temperature. The cores of the symmetrical dual vortex and high temperature region move to the sides of dimple when the Reynolds number increases. The temperature shows symmetrical distribution in different dimple depths when Re = 1000. However, the limiting streamline shows asymmetrical distribution when $\delta/D = 0.3$, which results from a large vortex existing in the leading edge of the dimple. As the Reynolds number increases, the cores of high temperature region becomes asymmetrical in both $\delta/D = 0.2$ and $\delta/D = 0.3$. At the same time, the dual vortex shows asymmetrical distribution when the Reynolds number is larger than 2000 in $\delta/D = 0.2$. It is noteworthy that the overall temperature decreases as Reynolds number increase in Figure 7, which has different legends in different Reynolds numbers.

4.2. Heat Transfer and Friction Characteristics. The ten dimple regions shows different flow characteristics and the conclusion could be drawn that the heat transfer in the ten dimple regions also show a big difference. Figure 8 presents the averaged Nusselt number distributions on the different dimple surfaces with the change of dimple depth and Reynolds number. The averaged Nusselt number decreases monotonously in the streamwise direction with Re = 1000 and Re = 2000 and the magnitudes are almost the same in different dimple depths, which results from that the flow is still laminar. Although the dimple introduces the vortex generator into main flow, it is not enough to change the overall laminar flow condition. As the Reynolds number increasing, the flow gradually transits into turbulent flow. The averaged Nusselt number in the streamwise direction shows the significant difference for cases with Re = 3000, 4000, and 5000. The averaged Nussselt number shows the similar trend when $\delta/D = 0.1$ and 0.2 with Re = 3000 as the cases of Re = 2000 while it decreases firstly and then increases from D6 region when $\delta/D = 0.3$ with Re = 3000, which indicates that the flow is transited from laminar to turbulent when the flow passes across D6 region. The averaged Nusselt number decreases monotonously in the streamwise direction when $\delta/D = 0.1$ with Re = 4000 while it starts to increase from D4 region when $\delta/D = 0.2$ and 0.3. The averaged Nusselt number decreases firstly and then increases with Re = 5000 in all dimple depths. The position at which the averaged Nusselt

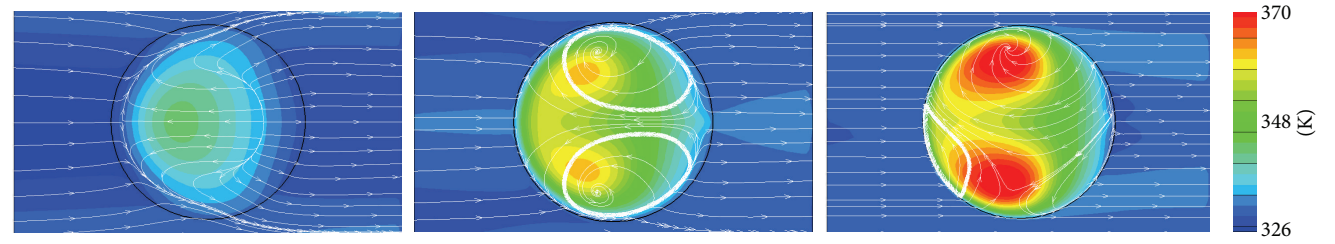

(a) Re = 1000

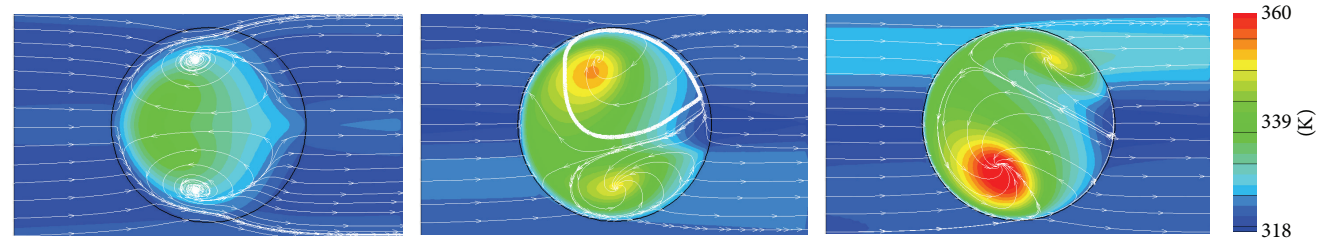

(b) Re = 2000

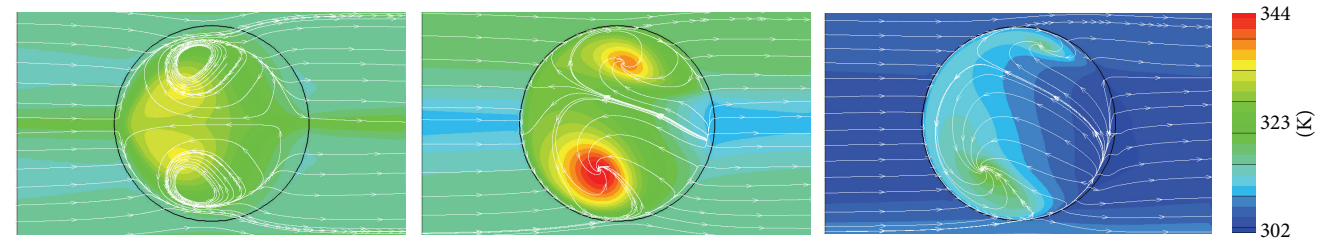

(c) Re = 3000

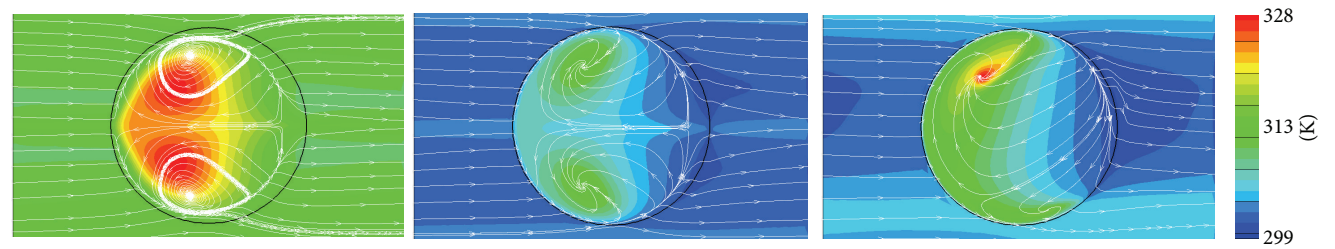

(d) Re = 4000

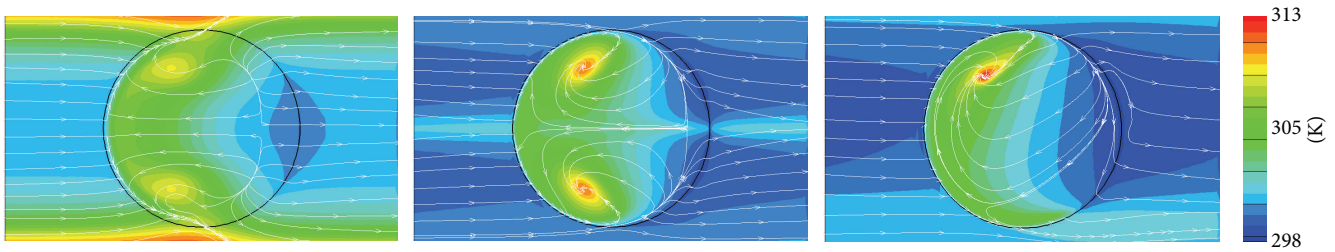

(e) Re = 5000

Figure 7: Limiting streamline and temperature distributions on dimple D10 region (left: $\delta/D = 0.1$, center: $\delta/D = 0.2$, right: $\delta/D = 0.3$).

number begins to increase is D6 region for $\delta/D = 0.1$ and D3 region for $\delta/D = 0.2$ and 0.3.

For better comparison of heat transfer enhancement between dimple cases and flat cases, the normalized averaged Nusselt number distributions in each dimple region with different dimple depth and Reynolds number are presented in Figure 9. The averaged Nusselt number for each dimple region in dimple cases is lower than that for the corresponding region in flat cases with Re = 1000 and 2000. Similarly, the averaged Nusselt number for the first three dimple regions

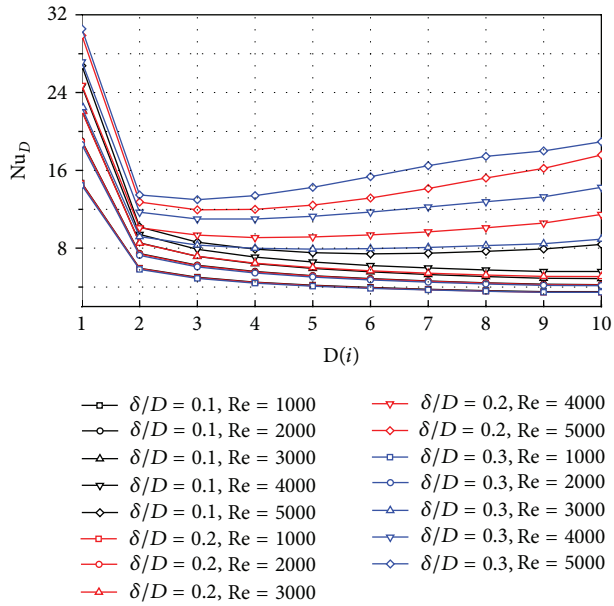

Figure 8: Averaged Nusselt number in each dimple region.

is slightly lower than that for the corresponding region in flat cases while it is higher for the other dimple regions with $\delta/D = 0.1$, 0.2 and Re = 3000. In the cases with Re = 4000 and 5000, the averaged Nusselt number is higher for each dimple region than that in flat cases as well as the case with Re = 3000 with $\delta/D = 0.3$. And the normalized averaged Nusselt number increases monotonously as the flow develops in the streamwise direction. It can be also found that the normalized averaged Nusselt number gets larger when the dimple depth becomes deeper. So the conclusion can be drawn that the flow transition is helpful for the heat transfer enhancement.

The normalized overall averaged Nusselt number variations with Reynolds number are shown in Figure 10. The normalized overall averaged Nusselt number increases significantly with the variation of Reynolds number from 4000 to 5000 for $\delta/D = 0.1$, from 3000–4000 for $\delta/D = 0.2$, and from 2000–3000 for $\delta/D = 0.3$. The overall averaged Nusselt number with dimple is lower than that with flat surface when Re = 1000 and 2000, which indicates that heat transfer is worsened by arranging the dimple on the target surface when the flow is laminar. The deeper the dimple depth is, the better the heat transfer performance presented in the investigation is, which results from that the deeper dimple introduces more turbulence kinetic energy into main flow.

The normalized overall friction factor variations with Reynolds number are shown in Figure 11. The trends of the normalized overall friction factor variation are significantly different for different dimple depths. The argument that the friction factor increases with dimple depth is pretty easy to follow. However, friction factor for $\delta/D = 0.1$ is lower than that with flat target in the all adopted Reynolds number cases due to the dimple with depth of $\delta/D = 0.1$ interrupting the boundary layer and reducing the flow separation loss. Furthermore, the normalized overall friction factor decreases with Reynolds number. When the dimple depth is higher than 0.1, the normalized overall friction factor decreases when the Reynolds number varies from 1000 to 2000, which indicates that the friction factor with dimple depth of 0.2 and 0.3 gets lower with the increasing of Reynolds number. The normalized overall friction factor increases with large degree when the Reynolds number is higher than 3000 and the value is up to 1.49 and 1.94 for $\delta/D = 0.2$ and $\delta/D = 0.3$, respectively.

4.3. Thermal Performance. Figure 12 compares the overall thermal performance characteristics as dependent upon Reynolds number with different dimple depths. Clearly, the overall thermal performance increases with Reynolds number, especially in the range of 4000–5000 for $\delta/D = 0.1$, 3000–4000 for $\delta/D = 0.2$ and 2000–3000 for $\delta/D = 0.3$ corresponding to the variations of nominal averaged Nusselt number. One point that can be predictable is that the overall thermal performance of dimple arrangement is near 1 when the flow is laminar and the overall thermal performance decreases with the increase of dimple depth. Furthermore, the overall thermal performance shows bigger value when the flow comes into turbulent condition. When the flow is fully developed, the case with $\delta/D = 0.2$ shows the best overall thermal performance which is as high as 1.85 in the comparison among different dimple depths.

5. Conclusions

Three-dimensional N-S equations were solved by SST turbulent model coupled with Gamma-Theta transition model, and the flow and heat transfer characteristics of a rectangular channel with arrays of dimples among transitional Reynolds number were firstly investigated in the present study.

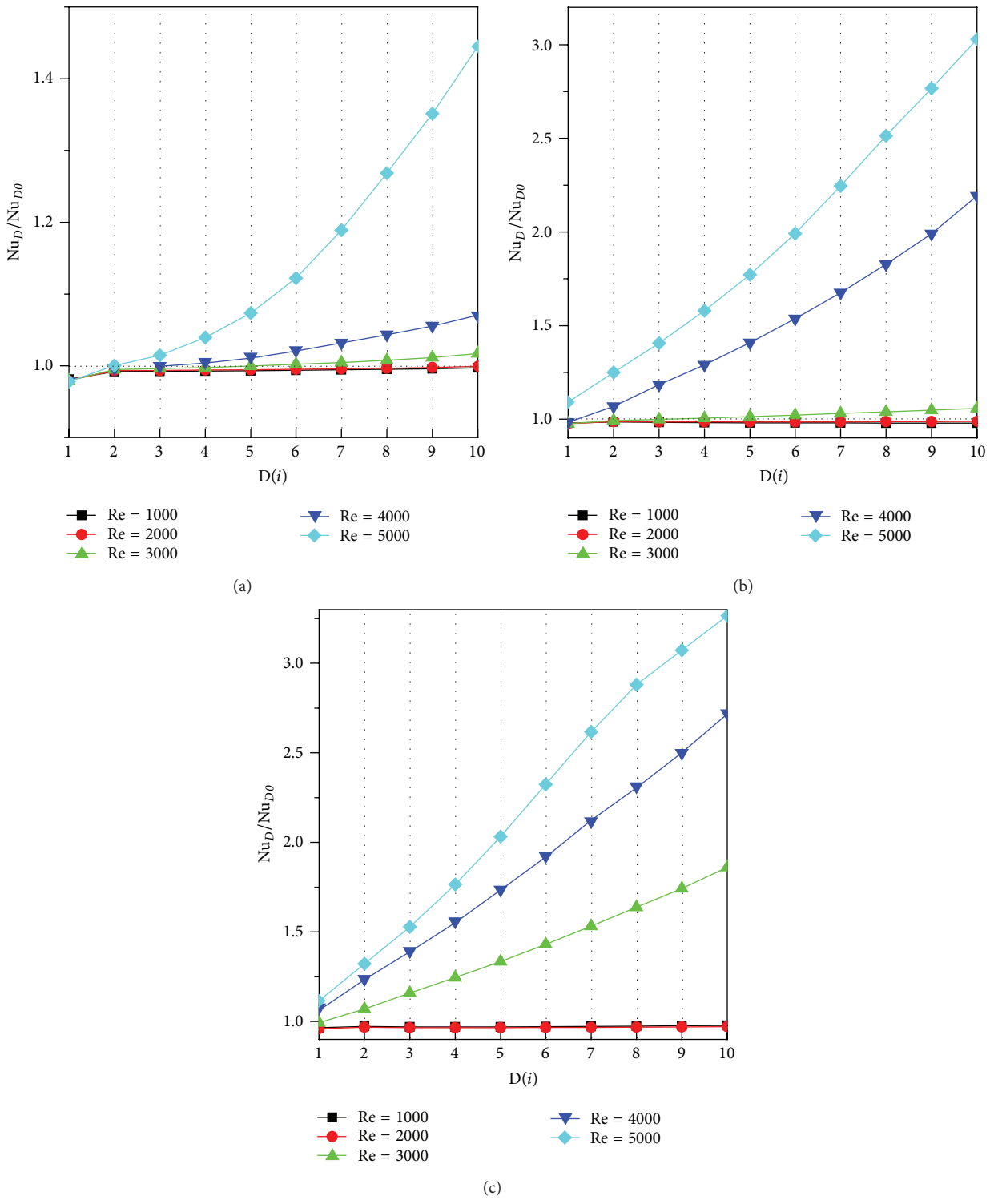

FIGURE 9: Normalized averaged Nusselt number in each dimple region ((a): $\delta/D = 0.1$, (b): $\delta/D = 0.2$ and (c): $\delta/D = 0.3$).

The dimple depth varies from 0.1 to 0.3 with variations of Reynolds number from 1000 to 5000. Grid independence validation was performed through four sets of grid system and the results shows that the adopted grid is sufficient for the computation. The numerical results show the following.

(1) The impact of dimple arrangement on velocity profile is different for variable Reynolds numbers. The velocity gets plumper along streamwise direction which indicates that the flow is transited from laminar flow to turbulent flow, which is also confirmed

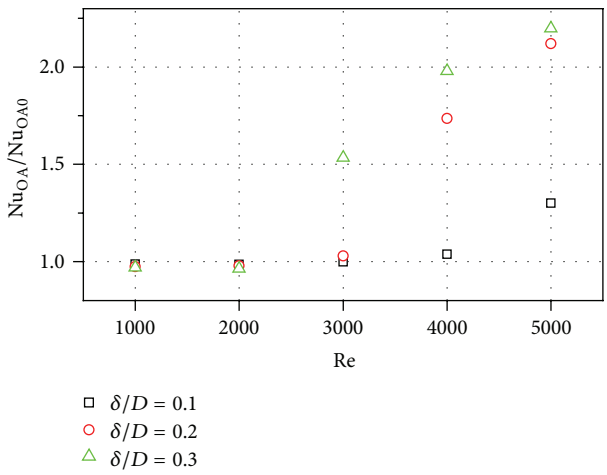

Figure 10: Normalized overall averaged Nusselt number variations with Reynolds number.

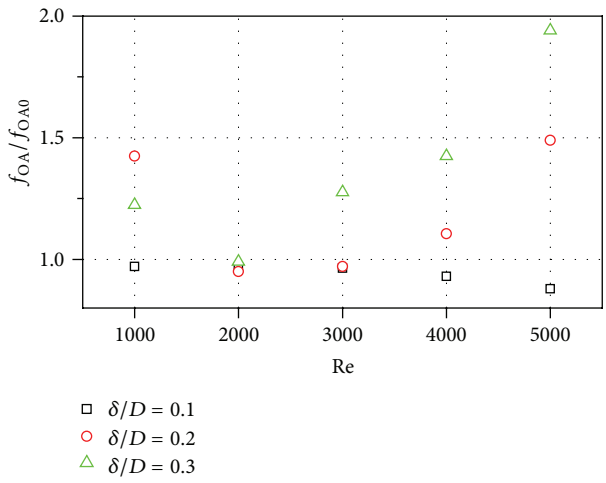

Figure 11: Normalized overall friction factor variations with Reynolds number.

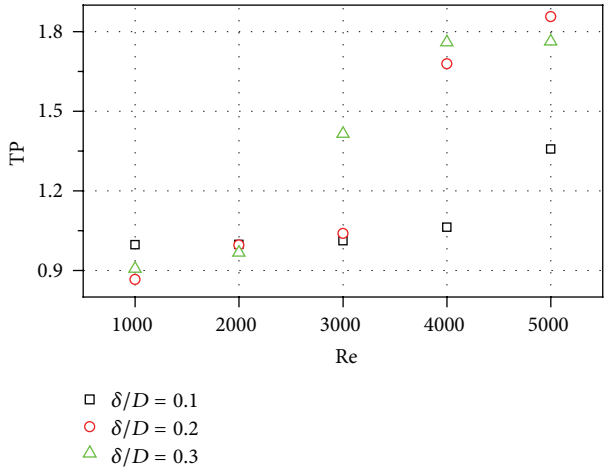

Figure 12: Overall thermal performance variations with Reynolds number.

by the turbulence intermittency distribution. Symmetrical dual vortex exists inside the dimple when Reynolds number is low. The dual vortex becomes asymmetrical when Reynolds number increases. The averaged Nusselt number decreases monotonously in the streamwise direction when the flow is under laminar condition while it increases monotonously when the flow is under turbulent condition.

(2) The heat transfer is enhanced by the dimple when the flow is turbulent and it increases with the dimple depth. Nu_D/Nu_{D0} and Nu_{OA}/Nu_{OA0} are as high as 3.26 and 2.20 with Re = 5000 and 0.3 in the last dimple region, repectively. However, the heat transfer is worsened by the dimple when the flow is laminar.

(3) The friction for $\delta/D = 0.1$ is lower than that with flat case due to the dimple interrupting the boundary layer and reducing the flow separation loss. However, the friction increases when the dimple depth increases with Reynolds number higher than 2000. f_{OA}/f_{OA0} is up to 1.49 and 1.94 for $\delta/D = 0.2$ and $\delta/D = 0.3$, respectively.

(4) The overall thermal performance increases with Reynolds number, especially in the transitional range of 4000–5000 for $\delta/D = 0.1$, 3000–4000 for $\delta/D = 0.2$ and 2000–3000 for $\delta/D = 0.3$ corresponding to the variations of nominal averaged Nusselt number. The value is near 1 when the flow is laminar while it becomes much higher when the flow gets into turbulence, in which the case with $\delta/D = 0.2$ shows that the best overall thermal performance is as high as 1.85.

References

[1] V. I. Terekhov, S. V. Kalinina, and Y. M. Mshvidobadze, "Heat transfer coefficient and aerodynamic resistance on a surface with a single dimple," *Journal of Enhanced Heat Transfer*, vol. 4, no. 2, pp. 131–145, 1997.

[2] M. K. Chyu, Y. Yu, and H. Ding, "Heat transfer enhancement in rectangular channels with concavities," *Journal of Enhanced Heat Transfer*, vol. 6, no. 6, pp. 429–439, 1999.

[3] H. K. Moon, T. O'Connell, and B. Glezer, "Channel height effect on heat transfer and friction in a dimpled passage," *Journal of Engineering for Gas Turbines and Power*, vol. 122, no. 2, pp. 307–313, 2000.

[4] P. M. Ligrani, G. I. Mahmood, J. L. Harrison, C. M. Clayton, and D. L. Nelson, "Flow structure and local Nusselt number variations in a channel with dimples and protrusions on opposite walls," *International Journal of Heat and Mass Transfer*, vol. 44, no. 23, pp. 4413–4425, 2001.

[5] P. M. Ligrani, N. K. Burgess, and S. Y. Won, "Nusselt numbers and flow structure on and above a shallow dimpled surface within a channel including effects of inlet turbulence intensity level," *Journal of Turbomachinery*, vol. 127, no. 2, pp. 321–330, 2005.

[6] N. K. Burgess and P. M. Ligrani, "Effects of dimple depth on channel nusselt numbers and friction factors," *Journal of Heat Transfer*, vol. 127, no. 8, pp. 839–847, 2005.

[7] S. Y. Won, Q. Zhang, and P. M. Ligrani, "Comparisons of flow structure above dimpled surfaces with different dimple depths in a channel," *Physics of Fluids*, vol. 17, no. 4, Article ID 045105, 2005.

[8] S. Y. Won and P. M. Ligrani, "Flow characteristics along and above dimpled surfaces with three different dimple depths within a channel," *Journal of Mechanical Science and Technology*, vol. 21, no. 11, pp. 1901–1909, 2007.

[9] J. Park and P. M. Ligrani, "Numerical predictions of heat transfer and fluid flow characteristics for seven different dimpled surfaces in a channel," *Numerical Heat Transfer A*, vol. 47, no. 3, pp. 209–232, 2005.

[10] S. W. Chang, K. F. Chiang, T. L. Yang, and C. C. Huang, "Heat transfer and pressure drop in dimpled fin channels," *Experimental Thermal and Fluid Science*, vol. 33, no. 1, pp. 23–40, 2008.

[11] S. D. Hwang, H. G. Kwon, and H. H. Cho, "Heat transfer with dimple/protrusion arrays in a rectangular duct with a low Reynolds number range," *International Journal of Heat and Fluid Flow*, vol. 29, no. 4, pp. 916–926, 2008.

[12] H. Lienhart, M. Breuer, and C. Köksoy, "Drag reduction by dimples?—A complementary experimental/numerical investigation," *International Journal of Heat and Fluid Flow*, vol. 29, no. 3, pp. 783–791, 2008.

[13] S. S. Kore, V. J. Satishchandra, and K. S. Narayan, "Experimental investigations of heat transfer enhancement from dimpled surface in a channel," *International Journal of Engineering Science & Technology*, vol. 3, no. 8, pp. 6277–6234, 2011.

[14] G. Xie, B. Sundén, and Q. Wang, "Predictions of enhanced heat transfer of an internal blade tip-wall with hemispherical dimples or protrusions," *Journal of Turbomachinery*, vol. 133, no. 4, Article ID 041005, 9 pages, 2011.

[15] G. Xie, B. Sunden, and W. Zhang, "Comparisons of pins/dimples/protrusions cooling concepts for a turbine blade tip-wall at high Reynolds numbers," *Journal of Heat Transfer*, vol. 133, no. 6, Article ID 061902, 9 pages, 2011.

[16] Y. Chen, Y. T. Chew, and B. C. Khoo, "Enhancement of heat transfer in turbulent channel flow over dimpled surface," *International Journal of Heat and Mass Transfer*, vol. 55, no. 25-26, pp. 8100–8121, 2012.

[17] Y. Rao, C. Wan, and S. Zang, "An experimental and numerical study of flow and heat transfer in channels with pin fin-dimple combined arrays of different configurations," *Journal of Heat Transfer*, vol. 134, no. 12, Article ID 121901, 11 pages, 2012.

[18] Y. Rao, Y. Xu, and C. Wan, "An experimental and numerical study of flow and heat transfer in channels with pin fin-dimple and pin fin arrays," *Experimental Thermal and Fluid Science*, vol. 38, pp. 237–247, 2012.

[19] Y. Rao, Y. Xu, and C. Wan, "A numerical study of the flow and heat transfer in the pin fin-dimple channels with various dimple depths," *Journal of Heat Transfer*, vol. 134, no. 7, Article ID 071902, 9 pages, 2012.

[20] E. Y. Choi, Y. D. Choi, W. S. Lee, J. T. Chung, and J. S. Kwak, "Heat transfer augmentation using a rib-dimple compound cooling technique," *Applied Thermal Engineering*, vol. 51, no. 1-2, pp. 435–441, 2013.

[21] C. Bi, G. H. Tang, and W. Q. Tao, "Heat transfer enhancement in mini-channel heat sinks with dimples and cylindrical grooves," *Applied Thermal Engineering*, vol. 55, no. 1-2, pp. 121–132, 2013.

[22] N. Xiao, Q. Zhang, P. M. Ligrani, and R. Mongia, "Thermal performance of dimpled surfaces in laminar flows," *International Journal of Heat and Mass Transfer*, vol. 52, no. 7-8, pp. 2009–2017, 2009.

[23] J. B. Lan, Y. H. Xie, and D. Zhang, "Flow and heat transfer in microchannels with dimples and protrusions," *Journal of Heat Transfer*, vol. 134, no. 2, Article ID 021901, 2012.

[24] F. R. Menter, "Two-equation eddy-viscosity turbulence models for engineering applications," *AIAA journal*, vol. 32, no. 8, pp. 1598–1605, 1994.

[25] F. R. Menter, R. B. Langtry, S. R. Likki, Y. B. Suzen, P. G. Huang, and S. Völker, "A correlation-based transition model using local variables—part I: model formulation," *Journal of Turbomachinery*, vol. 128, no. 3, pp. 413–422, 2006.

[26] R. Shah and A. London, *Laminar Flow Forced Convection in Ducts: A Source Book For Compact Heat Exchanger Analytical Data*, vol. 1, Academic Press, New York, NY, USA, 1978.